North Atlantic Mesoscale Eddy Detection and Marine Species Distribution

by

Ango Chen-Tien Hsu

Date: May 2010

Approved:

_____

Patrick N. Halpin, Advisor

Masters project submitted in partial fulfillment of the requirements for

the Master of Environmental Management degree in

the Nicholas School of the Environment of

Duke University

ABSTRACT

An eddy detection workflow was developed and applied to reference series of delayed time maps of sea level anomaly (Ref DT-MSLA) published by Aviso Altimetry, France in the North Atlantic region between 30-55° N and 30-80° W. The eddy detection parameters, maximum/minimum Okubo-Weiss parameter to assign to the eddy core/ring, minimum eddy core area, minimum eddy core area to perimeter ratio, and minimum eddy duration, were set to -0.2/0.2 standard deviation, 5 cells (6869 km^2), 0.4, and 10 images (70 days), respectively. Using these parameters, 635 anticyclonic eddies and 930 cyclonic eddies were detected between October 14, 1992 and December 31, 2005. The eddy structure of the 62103 pelagic longline fishery catch records in The Logbook System maintained by Southeast Fisheries Science Center was sampled. One-way ANOVA and t-test were conducted to compare the mean catch-per-unit-effort (CPUE) of bluefin tuna (*Thunnus thynnus*), yellowfin tuna (*Thunnus albacores*), bigeye tuna (*Thunnus obesus*), and swordfish (*Xiphius gladius*) at different eddy structures. For bluefin tuna and bigeye tuna, the mean CPUE is higher in the eddy area than in the non-eddy area. For yellowfin tuna and swordfish, the mean CPUE is higher in the non-eddy area than in the eddy area. For all three species of tuna, the mean CPUE is higher in the anticyclonic eddies than in the cyclonic eddies. For swordfish, the mean CPUE is higher in the cyclonic eddies than in the anticyclonic eddies. The results suggest different eddy structures make different habitats for large marine predators and eddy activities contribute to marine species distribution.

ACKNOWLEDGEMENT

The project would not have succeeded without the extensive support and help I received from many people. My thanks to all of you and to those I forgot to mention. Thanks to Dr. Pat Halpin, my research advisor, for supporting this project, introducing me to the world of GIS, and many opportunities he offered in the past two years. I learned a lot through those opportunities and I feel that somehow changed my life. Thanks to Jason Roberts for spending countless hours talking to me on Skype and patiently teaching me all kinds of knowledge in remotely sensed oceanographic data, different software packages, and programming in the past two years. Jason is a significant part of my Nicholas School experience. Thanks to Dr. Andre Boustany for sharing the fishery catch data and his knowledge in marine biology. Thanks to Dr. Paul Baker, my academic advisor, for being in charge of me since the first day I switched to GEC which is my second day at the Nicholas School. Thanks to Dr. Susan Lozier for a great class in fluid dynamics which helped the progress of this project. Thanks to John Fay for his help in geoprocessing scripts using Python. Thanks to all my colleagues and friends and administrative staffs in the Nicholas School for making me two great years. Thanks to Janice for her encouragement and the happiness she brings to my life. A special thank to my family, especially my parents, for their nonstop support, both financial and spiritual. They are, to most extent, the most important part of my life.

Table of Contents

Introduction

Eddies, or vortices, are nonlinear ocean mesoscale (scales of tens to hundreds of kilometers and tens to hundreds of days) variability. At the eddy center, the eddy core, vorticity dominates. The eddy ring, which surrounds the eddy core, experiences high rate of strain. According to oceanographers, eddy core is often comprises 50% to 60% diameter of the entire eddy (Henson and Thomas 2008). Eddies occur in every ocean on Earth, including Arctic and Antarctic regions. Mesoscale eddies occur when there is a balance between two major forces, horizontal pressure gradient force arising from differences in water density and the Coriolis force associated with the Earth's rotation (University of Hawaii website, www.geol.sc.edu/cbnelson/Eddy/index.htm). Other eddy formation mechanisms include currents moving vertically or flowing over seamounts, Rossby waves which travel westward over planetary scale, and spatial variation of water temperature. In the study area of this project, the North Atlantic region, the flow instabilities of the Gulf Stream pinches off relatively warm or cool waters that act as seeds for eddies. Eddies are generated at both sides of the current as the filaments of the current deform. Convergence and divergence of upper ocean waters produced by winds can also create eddies. The diameters of eddies vary from a few centimeters to hundreds of kilometers. Some eddies disappear soon after its generation while some can last months to years. Depending on the direction of rotation, eddy has two polarities, anticyclonic and cyclonic. In the northern hemisphere, anticyclonic eddy rotate clockwise and cyclonic eddy rotates counter-clockwise. The rotation directions of both anticyclonic eddy and cyclonic eddy reverse in the southern hemisphere. For both anticyclonic eddy and cyclonic eddy, centrifugal force points outward. The Coriolis force, which usually

outweighs centrifugal force, points inward in the anticyclonic eddy and outward in the cyclonic eddy. In the anticyclonic eddy, excess inward directed force drives water toward the interior of the eddy, increases the hydrostatic pressure, and creates downwelling at the eddy core. The eddy core of anticyclonic eddy appears as clustered positive cells on sea level anomaly maps since high hydrostatic pressure is created. We refer anticyclonic eddy as the warm ring because its downwelling at the eddy core which often traps warm water. In contrast, in the cyclonic eddy, excess outward directed force drives water outward the interior of the eddy, decreases the hydrostatic pressure, and forces the eddy core to upwell. The eddy core of cyclonic appears as clustered negative cells on sea level anomaly maps since low hydrostatic pressure is created. We refer cyclonic eddy as the cold ring because it upwells at the eddy core and brings relatively cool water from bottom of the ocean. The downwelling and upwelling characteristics at the eddy core of anticyclonic eddy (warm ring) and cyclonic eddy (cold ring) apply to both hemispheres (Bakun 2006).

The kinetic energy of mesoscale variability is more than an order of magnitude greater than the mean kinetic energy over most of the ocean (Wyrtki et al. 1976; Richardson 1983). Eddies are rotating water masses that contribute to the general circulation, large-scale water mass distributions, and ocean biology because of their effectiveness in transporting momentum, heat, mass, chemical constituents, and nutrients and their impact on mixing (Olson 1991; Chelton et al. 2007). At the center of a cyclonic eddy, freshly upwelled cool, nutrient-rich waters are a feast for phytoplankton. On the other hand, the anticyclonic eddy draws and aggregates water and materials from the ambient environment to form a highly concentrated area of these materials at its center. Many

research had shown that eddy activities affect water temperature (Gasca 2003a), nutrient cycling (McGillicuddy et al. 2003), phytoplankton and zooplankton assemblage (Paterson et al. 2007), the distribution and abundance of hyperiid amphipods (Gasca 2003b), sardine larvae survival (Logerwell et al. 2001), and fish distribution (Brandt 1981). The above facts led me to assume eddy activities affect the distribution of large predators in the marine ecosystem and these predators consider different eddy structures (eddy core; eddy ring) and different eddy polarities (anticyclonic eddy; cyclonic eddy) different habitats.

The project has two objectives. The first objective is to develop a workflow to detect eddy structures on time series sea level anomaly maps with the help of software packages such as Matlab, ArcGIS, and Python. An existing eddy core detection tool was applied in the North Atlantic region looking for eddy cores on 14 year (Oct. 1992 to Dec. 2005) time series sea level anomaly maps. The detected eddy cores were then buffered proportionally and eddy rings were searched within the buffer with a Python script that I composed. The second objective is to determine if eddy activities affect marine species distribution. I analyze a pelagic longline fishery catch dataset presented in The Logbook System with the detected eddy structures. I calculated catch-per-unit-effort (CPUE) of four large marine predator species, bluefin tuna (*Thunnus thynnus*), yellowfin tuna (*Thunnus albacores*), bigeye tuna (*Thunnus obesus*), and swordfish (*Xiphius gladius*), by dividing the number of fish caught of each species by the number of hook set at each catch point and conducted one-way ANOVA and t-test to compare if mean CPUE of each species is significantly different at different eddy structures or at eddy structure with different polarities. In this project, I focused on eddies which have a diameter of hundreds

of kilometers and last for months because those small and short lived eddies are not likely to be important to marine species distribution.

Methods

Sea Level Anomaly Maps

The remotely sensed dataset I worked with to detect eddies is delayed time map of sea level anomaly (DT-MSLA) published by Aviso Altimetry, France. The Doris System accurately tracks the position of an altimetry satellite based on the Doppler Effect. With position information of the satellite, the height of the satellite to a reference ellipsoid can be determined. By transmitting radar pulse to earth and measuring satellite-to-surface round-trip time of the pulse, the distance between satellite and sea surface is calculated. Sea surface height is derived by subtracting the distance between satellite and sea surface from height of the satellite. The dataset is accurate to a degree of a few centimeters. The dataset is ongoing and the earliest data goes back to September 1992. The spatial resolution and time resolution of the dataset are 37 kilometers and 7 days, respectively. For every seven days, we have a gridded sea level anomaly computed with respect to a seven-year mean covering the entire globe. DT-MSLA sea level anomalies have two sub-datasets, reference series (Ref) and updated series (Upd). I worked with reference series sub-dataset since it always averages measurements of two satellites with the same ground track, hence the reference series sub-dataset set is homogeneous through time. Depending on different time periods, the two satellites could be Topex/Poseidon/ERS, Jason-1/Envisat, or Jason-2/Envisat. In contrast, update series keeps adding measurements of up to four different satellites whenever a new satellite becomes available. Although update series provides more and more accurate measurements with increased satellite number, it would give non-homogeneous information of sea level anomaly throughout the images I detect eddy structures on. One advantage of sea level anomaly maps is radar pulse isn't

affected by clouds. I needn't to deal with clouds in this project since there won't be cloud contamination on the satellite images.

I downloaded reference series delayed time map of sea level anomaly (Ref DT-MSLA) between October 1992 and December 2005, clipped the downloaded images to an extent of the study area, the North Atlantic region between 30-55° N and 30-80° W, and fed the clipped images as the inputs of the workflow of detecting eddy structures on time series sea level anomaly maps. Figure 1 is an example of global extent sea level anomaly map on January 3rd, 2007. The black box on the figure depicts the extent of the study area. Figure 2 is the same image clipped to the North Atlantic region which has the extent within which I detected eddies in this project. Both images are in a Mercator projection with geographic coordinate system, datum, and spheroid defined by Aviso Altimetry.

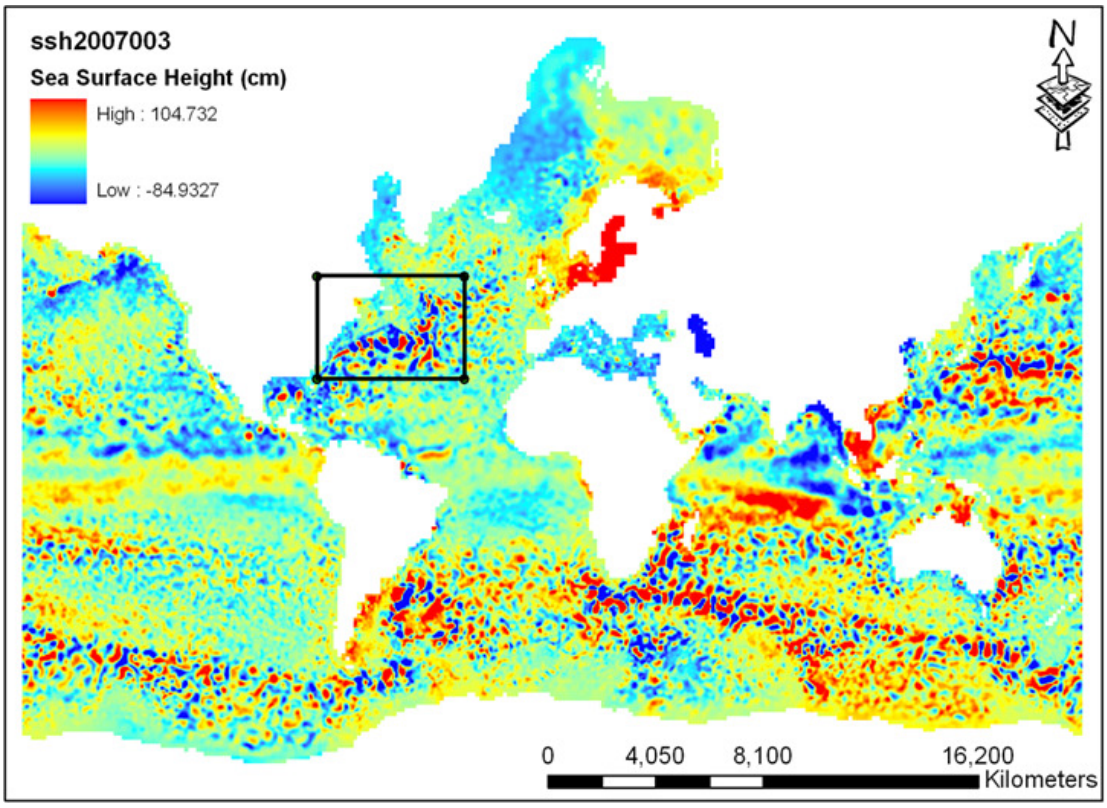

Figure 1. Global extent sea level anomaly map on January 3rd, 2007. The black box on the figure depicts the extent of the study area, the North Atlantic region.

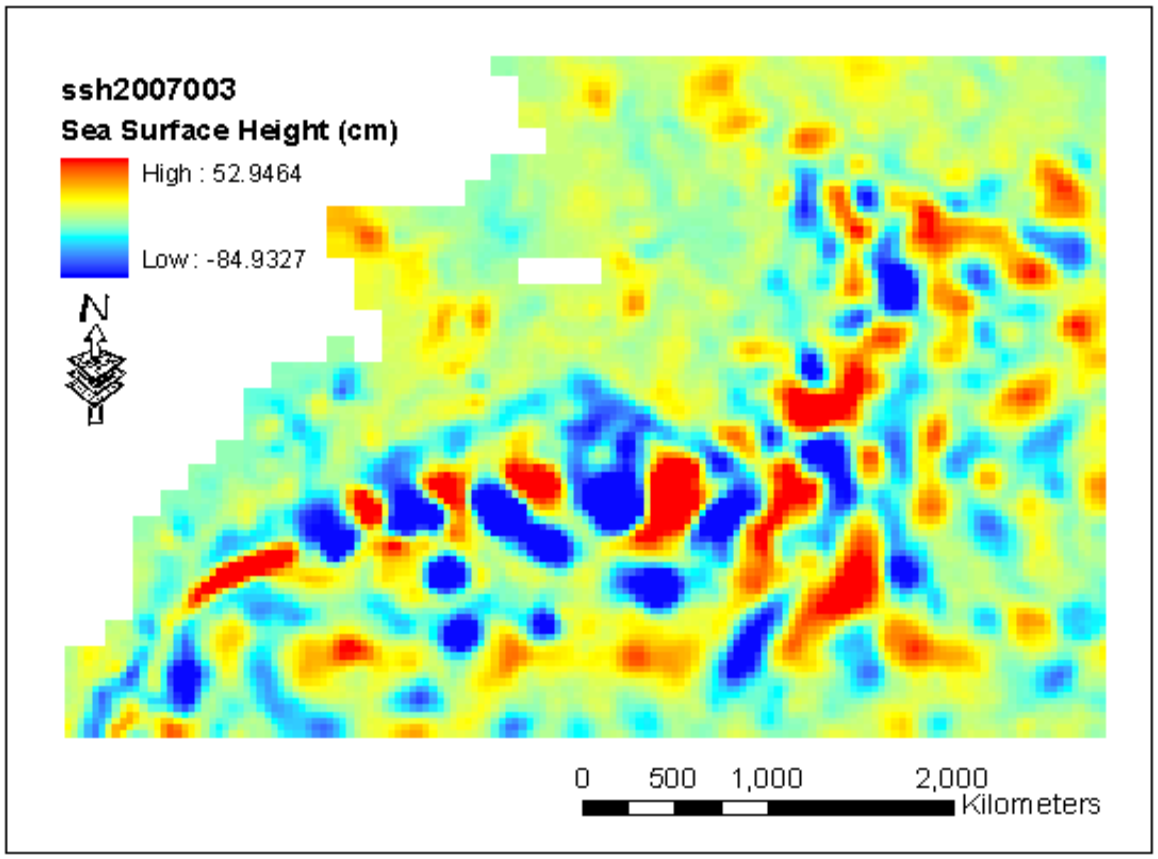

Figure 2. The same image as Figure 1 clipped to the extent of the study area, the North Atlantic region.

Eddy Detection

The Okubo-Weiss parameter, W, is often used to identify eddies in two-dimension sea level anomaly maps. The Okubo-Weiss parameter is defined as the normal component of strain (s_n^2) plus the shear component of strain (s_s^2) minus vorticity (ω^2), $W = s_n^2 + s_s^2 - \omega^2$. Dominated by vorticity, eddy core has large negative Okubo-Weiss parameter. In contrast, eddy ring, which is dominated by strain, has large positive Okubo-Weiss parameter. Henson and Thomas (2008) showed this relationship between eddy core, eddy ring, and the Okubo-Weiss parameter with a transect which runs through a mesoscale marine eddy (Figure 3; Henson and Thomas 2008).

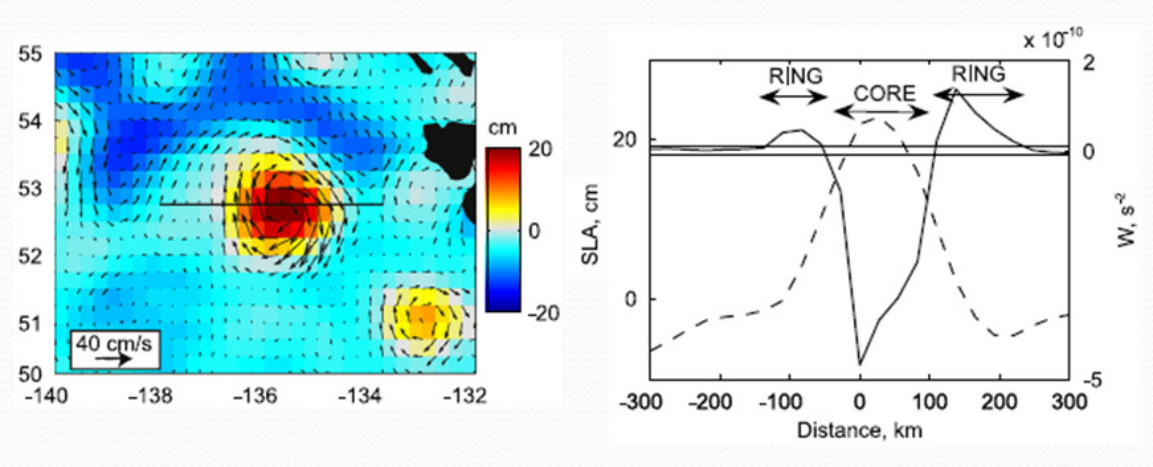

Figure 3. Plot of a transect which runs through an eddy against the Okubo-Weiss parameter (solid line in the right panel). The plot shows the eddy core has large negative Okubo-Weiss parameter while the eddy ring has the large positive Okubo-Weiss parameter.

Along with some other 200 tools, an existing eddy core detection tool is contained in Marine Geospatial Ecology Tools (MGET). Also known as GeoEco python package, MGET is an open source geoprocessing toolbox designed for coastal and marine researchers and GIS analysts who work with spatially-explicit ecological and oceanographic data (Roberts et al.). The eddy core detection tool MGET contains is a Matlab code which is able to detect eddy cores on time series sea level anomaly maps. Current eddy core detection tool walks through a few steps on sea level anomaly maps before it is able to compute the Okubo-Weiss parameter and assign cells with large negative Okubo-Weiss parameter to eddy core. It starts with deriving the u component and the v component of the velocity field from sea level anomalies based on two equations, $\mathbf{u} = -\frac{g}{f}\frac{\partial h'}{\partial y}$ and $\mathbf{v} = -\frac{g}{f}\frac{\partial h'}{\partial x}$, in which h' is sea level anomaly, g is acceleration due to gravity, and f is Coriolis parameter. The tool further computes the normal component and the shear component of strain and vorticity from the u component and the

v component of the velocity field with the following equations: $s_n = \partial_x u - \partial_y v$, $s_s = \partial_x v + \partial_y u$, and $\omega = \partial_x v - \partial_y u$, to calculate the Okubo-Weiss parameter. Scientists have not reached a consensus on the threshold Okubo-Weiss parameter to assign to the eddy core and the eddy ring in the eddy identification research. Some oceanographers set maximum Okubo-Weiss parameter to $-0.2\sigma_\omega$ to assign to the eddy core, where σ_ω is the spatial standard deviation of the Okubo-Weiss parameter (Isern-Fontanet et al. 2006). Henson and Thomas set maximum Okubo-Weiss parameter to $-0.2\sigma_\omega$ to assign to the eddy core as well as minimum Okubo-Weiss parameter to $0.2\sigma_\omega$ to assign to the eddy ring (Henson and Thomas 2008). Chelton et al. (2007) picked $-2*10^{-12}s^{-2}$ as maximum Okubo-Weiss parameter to assign to the eddy core (Chelton et al. 2007). In this project, I set maximum Okubo-Weiss parameter to $-0.2\sigma_\omega$ to assign to the eddy core and minimum Okubo-Weiss parameter to $0.2\sigma_\omega$ to assign to the eddy ring.

Other than the maximum Okubo-Weiss parameter to assign to the eddy core, the eddy core detection tool takes another three input parameters, minimum eddy core area, minimum eddy core area to perimeter ratio (scaled such that perfect circular has a value of 1.0), and minimum eddy duration. To detect large, long lived eddies (hundreds of kilometers in diameter, lasting for months) which are likely to be important to marine species distribution, I tried different combinations of input parameters and compared the detected eddy cores to sea surface temperature images prepared by GOES 11 Satellite and GOES 12 Satellite to make sure the eddy core detection tool captures most of the eddy-like structures on the sea surface temperature images. I set the thresholds listed in Table 1 for the tool's input parameters to detect eddy cores in the North Atlantic region.

Table 1. Thresholds for input parameters set in the eddy core detection tool.

Tool input parameter	Threshold
Maximum Okubo-Weiss parameter to assign to eddy core	$-0.2\sigma_\omega$
Minimum eddy core area	5 cells = 6869 km^2
Minimum eddy core area to perimeter ratio	0.4
Minimum eddy duration	10 images = 70 days

The tool outputs detected eddy cores with metadata such as the polarity, whether the detected eddy cores are anticyclonic eddies or cyclonic eddies, and the age of the detected eddy cores on a particular image.

With a Python script that I composed, I buffered the detected eddy cores proportionally so the detected eddy cores comprise roughly 50% diameter of the buffers and search large positive Okubo-Weiss parameter, $0.2\sigma_\omega$, within the buffers to assign to the eddy ring. At the end of the eddy detection process, for every 7 days, I have polygon layers of anticyclonic eddy core, cyclonic eddy core, anticyclonic eddy ring, and cyclonic eddy ring that I used the catch points presented in the pelagic longline fishery catch dataset to sample with.

Pelagic Longline Fishery Catch Data

The pelagic longline fishery catch data I worked with is presented in The Logbook System and maintained by Southeast Fisheries Science Center. The data is ongoing and goes back to 1992. I used the data between October 1992 and December 2005 to match the start date of the sea level anomaly dataset. The data after 2005 of the fishery data hasn't been processed and cleaned, hence is hard to work with. The fishery catch data has some 160,000 catch points in between October 1992 and December 2005. After parsing out all the catch points which are outside the study area, the North Atlantic region between 30-55° N and 30-80° W, I was left with 62,121 catch points (Figure 4). At every

catch point, I have information of date, location (latitude and longitude), number of fish caught of each species, and number of hooks set. Table 2 is an example of a few rows of the fishery data. At each catch point, I calculated catch-per-unit-effort (CPUE) of each species by dividing the number of fish caught of each species by the number of hooks set. The reason that I must normalize number of fish caught by the number of hooks and analyze mean CPUE of each species with respect to different eddy structures is, if I see a high mean CPUE of a species at a particular eddy structure, I wouldn't know it's because of the eddy activities or it's because there is more fishing in the area.

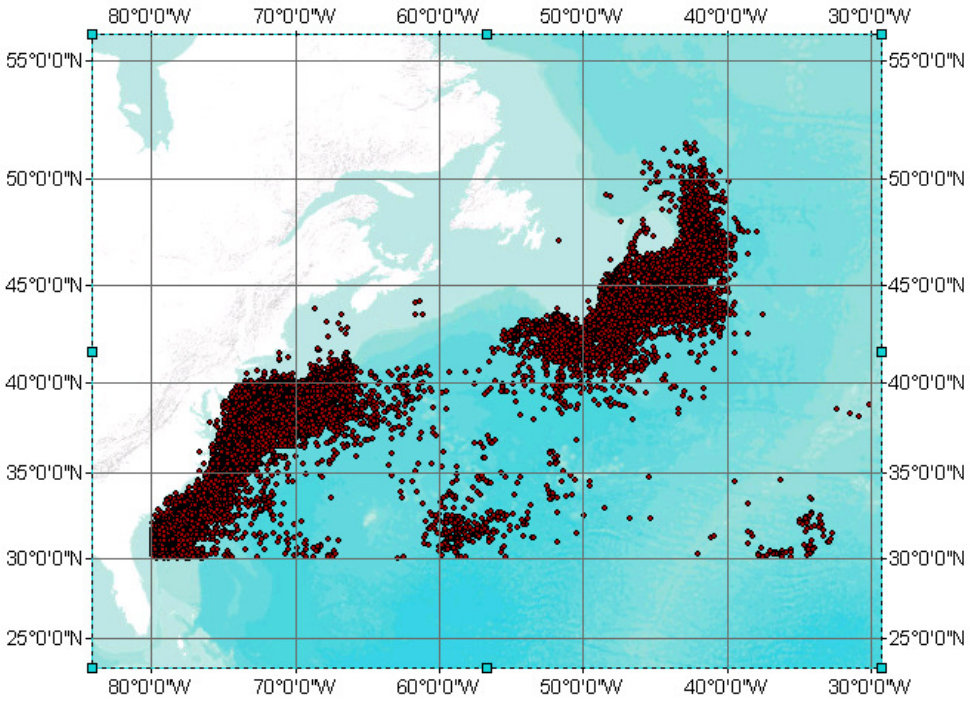

Figure 4. The 62,121 catch points presented in The Logbook System within the study area, the North Atlantic region.

Table 2. A few rows of the fishery catch data. At every catch point, I have information of date, latitude, longitude, number of swordfish (SWO), bigeye tuna (BET), bluefin tuna (BFT), and yellowfin tuna (YFT) caught, and number of hooks set.

C	D	E	F	G	H	I	J	K	L
YEAR_	MONTH_	DAY_	LAT	LON	HOOKS_SET	SWO	BET	BFT	YFT
1993	3	29	32.5	-75.5	878	3	0	0	8
1993	3	30	32.5	-75.5	779	5	0	0	3
1993	6	10	40.43	-66.5	600	6	2	1	1
1993	6	22	40.33	-66.5	600	8	0	9	0
1993	7	2	40.26	-66.5	400	11	7	0	5
1993	7	7	39.5	-67.5	300	1	0	0	0
1993	7	10	39.5	-67.5	300	0	0	0	2
1993	7	11	39.5	-67.5	300	1	0	0	0
1993	7	12	39.5	-67.5	300	1	1	0	0

Sampling

I sampled the distances each catch point to anticyclonic eddy core, to cyclonic eddy core, to anticyclonic eddy ring, and to cyclonic eddy ring with the help of the "Find Nearest Features Listed in Field" tool presented in MGET. I then determined the distance each catch point to eddy core by looking at the minimum distance between distance to anticyclonic eddy core and distance to cyclonic eddy core. Similarly, I determined the distance each catch point to eddy ring by looking at the minimum distance between distance to anticyclonic eddy ring and distance to cyclonic eddy ring. Finally I determined what eddy structure each catch point locates based on the information of these distances each catch point to different eddy structures that I sampled. Table 3 is a fictitious table which illustrates the sampling process.

Table 3. A fictitious table which illustrates the sampling process. Distance to anticyclonic eddy core (column M), to cyclonic eddy core (column N), to anticyclonic eddy ring (column O), to cyclonic eddy ring (column P) of each catch point were sampled. Distance of each catch point to eddy core (column Q) is determined by looking at the minimum between column M and N and distance of each catch point to eddy ring (column R) is determined by looking at the minimum between column O and P. Finally, which eddy structure each catch point locates was categorized.

M	N	O	P	Q	R	
ancoDist	cycoDist	anriDist	cyriDist	coreDist	ringDist	
1978273	414519.4	1897779	352129.5	414519.3	352129.5	← Non-eddy area
0	401807.5	1877967	330256.8	0	330256.8	← Anticyclonic eddy core
1949062	0	1869380	321910.9	0	321910.9	← Cyclonic eddy core
1932440	377321.5	0	305192	377321.4	0	← Anticyclonic eddy ring
1924172	370649.8	1844562	0	370649.7	0	← Cyclonic eddy ring
1892804	342851	0	0	342851	0	← Ring shared by both polarities
0	407653.1	0	333214.1	0	0	← Anticyclonic boundary
1475062	0	1406944	0	0	0	← Cyclonic boundary

Analysis

I compared the mean CPUE of the four marine species, bluefin tuna, yellowfin tuna, bigeye tuna, and swordfish, at different eddy structures and at eddy structure with different polarities. When more than two groups are involved, one-way ANOVA was conducted followed by a Bonferroni test to determine the mean CPUE of which two groups are significantly different at 95% confidence level. When the comparison involves only two groups, t-test was conducted.

Results and Discussion

Eddy Detection

With the input parameters of the eddy detection workflow setting to the thresholds described in the Methods session, 1565 eddy cores were detected between October 1992 and December 2005 in the North Atlantic region. Among which, 635 detected eddy cores are anticyclonic eddy cores and 930 detected eddy cores are cyclonic eddy cores. The eddy which has the longest duration survives 81 images (567 days). The image which has the most detected eddy cores has 47 detected eddy cores. Figure 5 is an example of detected eddy cores. All the detected anticyclonic eddy cores locate within the area of large positive sea level anomaly and all the detected cyclonic eddy cores locate within the area of large negative sea level anomaly. When overlapping with the direction and magnitude of the geostrophic current, clockwise rotation of the anticyclonic eddy core and counter-clockwise rotation of the cyclonic eddy core were observed.

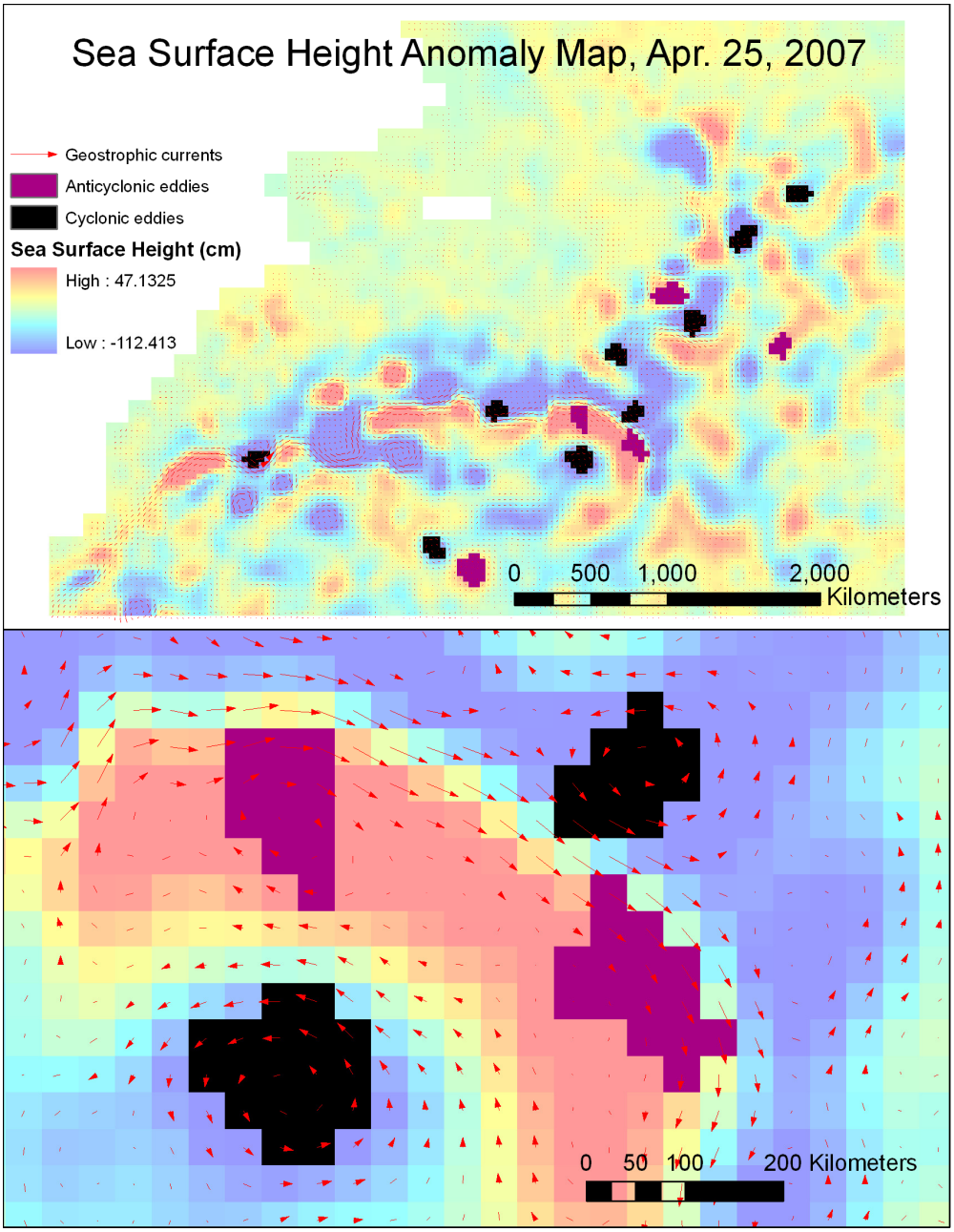

Figure 5. An example of detected eddy cores. Anticyclonic eddy cores locate within the area of large positive sea level anomaly and all cyclonic eddy cores locate within the area of large negative sea level anomaly. Anticyclonic eddy cores rotate clockwise and cyclonic eddy cores rotate counter-clockwise.

Sampling

I categorized the 62,121 catch points to the eddy structure they locate by looking at the information of their distances to different eddy structures that I sampled. 18 catch points

failed the sampling process. At the end of the sampling process, I have Table 4 which summarizes the number of catch points locating at different eddy structures. Most of the catch points locate in the non-eddy area. However, there are also some catch points which locate in the eddy core or the eddy ring of different polarities.

Table 4. Summary table of the number of catch points locating at different eddy structures.

Eddy structure	Records	Eddy polarity	Records
Eddy core	573	Anticyclonic eddy core	472
		Cyclonic eddy core	101
Eddy ring	2845	Anticyclonic eddy ring	2487
		Cyclonic eddy ring	335
		Ring shared by both polarities	23
Core ring boundary	72	Anticyclonic boundary	56
		Cyclonic boundary	16
Non-eddy area	58613		
Total	62103		

Marine Species Distribution

For all the tables below, P-values shaded blue denote the relationship is statistically significant at 95% confidence level. Superscript red numbers denote ranking among the row with 1 representing the highest rank, 2 representing the second highest rank, and so on. Mean CPUE shaded in red is the number with higher value among the row when only two groups are involved in the comparison.

A few one-way ANOVA tests were performed to test if the mean CPUE of each of the four species, bluefin tuna, yellowfin tuna, bigeye tuna, and swordfish, at different eddy structures are significantly different from each other. The mean CPUE of each species at different eddy structures and the F-statistics of these one-way ANOVA tests are listed in Table 5. The F-statistics in Table 5 suggest, for all four species, the mean CPUE at at least two eddy structures are significantly different at 95% confidence level. To probe the

mean CPUE of these species at which eddy structures are different, I conducted Bonferroni tests on each one-way ANOVA test and listed P-values of these tests in Table 6.

Table 5. Mean CPUE of different species at different eddy structures and the F-statistics of one-way ANOVA tests.

	Eddy core	Eddy ring	Core ring boundary	Non-eddy area	Pr(>F)
Mean CPUE bluefin	[4]$1.735*10^{-4}$	[1]$4.988*10^{-4}$	[3]$2.905*10^{-4}$	[2]$3.111*10^{-4}$	0.0109
Mean CPUE yellowfin	[2]$6.001*10^{-3}$	[3]$5.948*10^{-3}$	[4]$5.700*10^{-3}$	[1]$7.794*10^{-3}$	0.0000
Mean CPUE bigeye	[3]$5.311*10^{-3}$	[2]$5.756*10^{-3}$	[1]$5.883*10^{-3}$	[4]$3.279*10^{-3}$	0.0000
Mean CPUE swordfish	[2]$11.71*10^{-3}$	[3]$9.183*10^{-3}$	[4]$8.765*10^{-3}$	[1]$14.03*10^{-3}$	0.0000

Table 6. P-values of Bonferroni tests on one-way ANOVA tests in Table 5.

P-value	Eddy ring	Core ring boundary	Non-eddy area
Eddy core			
Mean CPUE bluefin	0.133	1.000	1.000
Mean CPUE yellowfin	1.000	1.000	0.071
Mean CPUE bigeye	1.000	1.000	0.000
Mean CPUE swordfish	0.019	1.000	0.018
Eddy ring			
Mean CPUE bluefin		1.000	0.010
Mean CPUE yellowfin		1.000	0.000
Mean CPUE bigeye		1.000	0.000
Mean CPUE swordfish		1.000	0.000
Core ring boundary			
Mean CPUE bluefin			1.000
Mean CPUE yellowfin			1.000
Mean CPUE bigeye			0.059
Mean CPUE swordfish			0.101

According to Table 6, for all four species, the mean CPUE at the core ring boundary is not significantly different from the mean CPUE at any other eddy structures at 95% confidence level. I then removed the catch records at the core ring boundary (72 records) from the following analyses. Notice that even before the removal of the boundary records, the mean CPUE at the eddy ring of all four species is considered statistically different from the mean CPUE at the non-eddy area. For bigeye tuna and swordfish, the mean CPUE at the eddy core is statistically different from the mean CPUE at the non-eddy area.

For swordfish, the mean CPUE at the eddy core is statistically different from the mean CPUE at the eddy ring which makes the mean CPUE of swordfish at the eddy core, at the eddy ring, and at the non-eddy area all different at 95% confidence level.

I conducted one-way ANOVA and Bonferroni tests on the mean CPUE of the four species at different eddy structures after the removal of the boundary records. The F-statistics and P-values of these tests are provided in Table 7 and Table 8. The difference of the mean CPUE at the eddy core and at the non-eddy area became statistically significant at 95% confidence level for yellowfin tuna after the boundary records were removed. Besides the differences in the mean CPUEs at the eddy ring and at the non-eddy area, which are statistically significant for all four species, the differences in the mean CPUE at the eddy core and at the non-eddy area are considered significant for almost all the species (except for bluefin tuna). For bluefin tuna and bigeye tuna, the mean CPUE is higher within the eddy area (at the eddy ring for bluefin tuna; both at the eddy core and at the eddy ring for bigeye tuna) than at the non-eddy area. For yellowfin tuna and swordfish, the mean CPUE is higher at the non-eddy area than within the eddy area. For swordfish, the mean CPUE is the highest at the non-eddy area followed by at the eddy core and is the lowest at the eddy ring.

Table 7. Mean CPUE of different species at different eddy structures and the F-statistics of one-way ANOVA tests after the boundary records were removed.

	Eddy core	Eddy ring	Non-eddy area	Pr(>F)
Mean CPUE bluefin	[3]$1.735*10^{-4}$	[1]$4.988*10^{-4}$	[2]$3.111*10^{-4}$	0.0038
Mean CPUE yellowfin	[2]$6.001*10^{-3}$	[3]$5.948*10^{-3}$	[1]$7.794*10^{-3}$	0.0000
Mean CPUE bigeye	[2]$5.311*10^{-3}$	[1]$5.756*10^{-3}$	[3]$3.279*10^{-3}$	0.0000
Mean CPUE swordfish	[2]$11.71*10^{-3}$	[3]$9.183*10^{-3}$	[1]$14.03*10^{-3}$	0.0000

Table 8. P-values of Bonferroni tests on one-way ANOVA tests in Table 7.

P-value	Eddy ring	Non-eddy area
Eddy core		
Mean CPUE bluefin	0.067	0.875
Mean CPUE yellowfin	1.000	0.035
Mean CPUE bigeye	0.769	0.000
Mean CPUE swordfish	0.010	0.009
Eddy ring		
Mean CPUE bluefin		0.005
Mean CPUE yellowfin		0.000
Mean CPUE bigeye		0.000
Mean CPUE swordfish		0.000

I combined the catch points at the eddy core and at the eddy ring to catch points at the eddy area in general and compared the mean CPUE of the four marine species at the eddy area to at the non-eddy area using t-tests. The results of these t-tests are provided in Table 9.

Table 9. Mean CPUE of different species at the eddy area and at the non-eddy area and the P-values of the t-tests.

	Eddy area	Non-eddy area	Pr(>|t|)
Mean CPUE bluefin	$4.411*10^{-4}$	$3.111*10^{-4}$	0.0006
Mean CPUE yellowfin	$5.952*10^{-3}$	$7.794*10^{-3}$	0.0000
Mean CPUE bigeye	$5.685*10^{-3}$	$3.279*10^{-3}$	0.0000
Mean CPUE swordfish	$9.589*10^{-3}$	$14.03*10^{-3}$	0.0000

According to Table 9, for bluefin tuna and bigeye tuna, the mean CPUE is higher within the eddy area than in the non-eddy area. However, for yellowfin tuna and swordfish, the mean CPUE is higher in the non-eddy area than within the eddy area. All of the relationships listed in Table 9 are statistically significant at 95% confidence level.

To determine if the polarity of eddy structure affects the distribution of marine species, I conducted a t-test for each species comparing the mean CPUE at the anticyclonic eddy core and at the cyclonic eddy core and provided the t-statistics of these tests in Table 10. Interestingly, all three tuna species seem to favor the anticyclonic eddy core than the

cyclonic eddy core while the swordfish's case appears to be the opposite. The difference in mean CPUE at eddy cores with different polarities is considered statistically significant at 95% confidence level for all four species.

Table 10. Mean CPUE of different species at eddy cores with different polarities and the P-values of the t-tests.

	Anticyclonic eddy core	Cyclonic eddy core	Pr(>|t|)
Mean CPUE bluefin	$20.00*10^{-5}$	$4.970*10^{-5}$	0.0152
Mean CPUE yellowfin	$6.551*10^{-3}$	$3.432*10^{-3}$	0.0107
Mean CPUE bigeye	$5.636*10^{-3}$	$3.795*10^{-3}$	0.0436
Mean CPUE swordfish	$1.067*10^{-2}$	$1.655*10^{-2}$	0.0004

I conducted similar t-tests to compare the difference in mean CPUE of these four marine species at eddy rings with different polarities and summarized the results and the P-values of these t-tests in Table 11.

Table 11. Mean CPUE of different species at eddy rings with different polarities and the P-values of the t-tests.

	Anticyclonic eddy ring	Cyclonic eddy ring	Pr(>|t|)
Mean CPUE bluefin	$5.302*10^{-4}$	$2.562*10^{-4}$	0.0003
Mean CPUE yellowfin	$5.972*10^{-3}$	$4.727*10^{-3}$	0.0942
Mean CPUE bigeye	$5.938*10^{-3}$	$4.600*10^{-3}$	0.0046
Mean CPUE swordfish	$7.829*10^{-3}$	$18.67*10^{-3}$	0.0000

Similar patterns were observed that all the tuna species favor anticyclonic eddy ring over cyclonic eddy ring while swordfish favors cyclonic eddy ring over anticyclonic eddy ring. All the differences in mean CPUE between eddy rings with different polarities are statistically significant at 95% confidence level except for the difference for yellowfin tuna, which is close to significant. If considering 90% confidence level, it would become significant.

I then combined the catch points at the anticyclonic eddy core and at the anticyclonic eddy ring to the catch points at the anticyclonic eddy in general as well as the catch

points at the cyclonic eddy core and at the cyclonic eddy ring to the catch points at the cyclonic eddy in general and compared mean CPUE of the four marine species at eddy area with different polarities using t-tests and provided the results and the P-values of these t-tests in Table 12. According to Table 12, all three tuna species favor anticyclonic eddy over cyclonic eddy while swordfish favors cyclonic eddy over anticyclonic eddy and all of these relationships are statistically significant at 95% confidence level.

Table 12. Mean CPUE of different species at eddies with different polarities and the P-values of the t-tests.

	Anticyclonic eddy	Cyclonic eddy	Pr(>|t|)
Mean CPUE bluefin	$4.775*10^{-4}$	$2.084*10^{-4}$	0.0000
Mean CPUE yellowfin	$6.064*10^{-3}$	$4.427*10^{-3}$	0.0173
Mean CPUE bigeye	$5.890*10^{-3}$	$4.413*10^{-3}$	0.0007
Mean CPUE swordfish	$8.282*10^{-3}$	$18.18*10^{-3}$	0.0000

In summary, comparing mean CPUE at the eddy area and at the non-eddy area, bluefin tuna and bigeye tuna favor eddy area over non-eddy area while yellowfin tuna and swordfish favor non-eddy area over eddy area. Comparing eddy area with different polarities, all three tuna species favor anticyclonic eddy over cyclonic eddy while swordfish favors cyclonic eddy over anticyclonic eddy. The marine species distribution patterns we observed could be potentially explained by looking at the animals' physiological limitation, cold tolerance for example, as well as their foraging behavior. The animal's cold tolerance depends on the size of the animal. Among these four species, bluefin tuna has the greatest cold tolerance followed by swordfish followed by bigeye tuna. Yellowfin tuna has the least cold tolerance. Also, bluefin tuna and yellowfin tuna are shallow feeder while bigeye tuna and swordfish are deep feeder. More literature review on marine biology is needed to hypothesize a more complete explanation of the species distribution patterns I observed in this project.

Future Research

I could change the combination of the input parameters of the eddy detection workflow. When the input parameters are changed, the workflow detects different eddy structures. If the marine species distribution patterns remain the same when I analyze them with different structures, we can further confirm that the patterns we observed are actually happening. If the distribution patterns changed, then we need to be very careful in defining eddies using different combinations of input parameters.

I can also use higher spatial resolution sea level anomaly maps to detect finer scale eddy structure. Hycom provides 3 time higher spatial resolution sea level anomaly maps than the Aviso images I worked with in this project. The disadvantage of using Hycom images is, instead of 14 years, it only provides 2 years of overlap with the fishery catch we currently have.

I could expand the study area to the southeast coast of the United States and Gulf Maxico. We have adequate sea level anomaly maps and fishery catch data to support such extent of studies.

Literature Cited

Bakun, A., 2006: Fronts and eddies as key structures in the habitat of marine fish larvae: opportunity, adaptive response and competitive advantage. *Scientia Marina,* 70S2, 105-122.

Brandt, S. B., 1981: Effects of a warm-core eddy on fish distributions in the Tasman Sea off East Australia. *Marine Ecology,* 6, 19-33.

Chelton, D. B., M. G. Schlax, R. M. Samelson, and R. A. de Szoeke, 2007: Global observations of large oceanic eddies. *Geophysical Research Letters,* 34, L15606, doi:10.1029/2007GL030812.

Gasca, R., 2003a: Hyperiid amphipods (Crustacea: Peracarida) in relation to a cold-core ring in the Gulf of Mexico. *Hydrobiologia,* 510, 115-124.

Gasca, R., 2003b: Hyperiid amphipods (Crustacea: Peracarida) and spring mesoscale features in the Gulf of Mexico. *Marine Ecology,* 24(4), 303-317.

Henson, S. A. and A. C. Thomas, 2008: A census of oceanic anticyclonic eddies in the Gulf of Alaska. *Deep Sea Research I,* 66, 163–176.

Isern-Fontanet, J., E. Garcia-Ladona, and J. Font, 2006: Vortices of the Mediterranean Sea: An altimetric perspective. *Journal of Physical Oceanography,* 36, 87-103.

Logerwell, E.A., and P. E. Smith, 2001: Mesoscale eddies and survival of late stage Pacific sardine (*Sardinops sagax*) larvae. *Fisheries Oceanography,* 10, 13-25.

McGillicuddy, D. J., and A. R. Robinson, 1997: Eddy induced nutrientsupply and new production in the Sargasso Sea. *Deep Sea Research I,* 44, 1427-1450.

Olson, D., 1991: Rings in the ocean. *Annual Review of Earth and Planetary Sciences,* 19, 283-311.

Paterson, H. L., B. Knott, and A. M. Waite, 2007: Microzooplankton community structure and grazing on phytoplankton, in an eddy pair in the Indian Ocean off Western Australia. *Deep Sea Research II,* 54, 1076-1093.

Richardson, P. L., 1983: Eddy kinetic energy in the North Atlantic Ocean from surface drifters. *Journal of Geophysical Research*, 88, 4355-4367.

Roberts, J. J., B. D. Best, D. C. Dunn, E. A. Treml, and P. N. Halpin, in press: Marine Geospatial Ecology Tools: An integrated framework for ecological geoprocessing with ArcGIS, Python, R, MATLAB, and C++. *Environmental Modelling & Software*.

Wyrtki, K., L. Magaard, and J. Hager, 1976: Eddy energy in the oceans. *Journal of Geophysical Research*, 81, 2641-2646.